Published in final edited form as:
Nat Photonics. 2015 July ; 9(7): 444–449. doi:10.1038/nphoton.2015.82.

Detection of X-ray photons by solution-processed organic-inorganic perovskites

Sergii Yakunin[1,2], **Mykhailo Sytnyk**[1], **Dominik Kriegner**[1], **Shreetu Shrestha**[3], **Moses Richter**[3], **Gebhard J. Matt**[3], **Hamed Azimi**[3], **Christoph J. Brabec**[3,4], **Julian Stangl**[1], **Maksym V. Kovalenko**[2,5], and **Wolfgang Heiss**[1,3,4,*]

[1]Institute of Semiconductor and Solid State Physics, University Linz, Altenbergerstraße 69, Linz 4040 Austria [2]Institute of Inorganic Chemistry, Department of Chemistry and Applied Biosciences, ETH Zürich, CH-8093 Zürich, Switzerland [3]Materials for Electronics and Energy Technology (i-MEET), Friedrich-Alexander-Universität Erlangen-Nürnberg, Martensstraße 7, 91058 Erlangen, Germany [4]Energie Campus Nürnberg (EnCN), Fürther Straße 250, 90429 Nürnberg, Germany [5]Empa – Swiss Federal Laboratories for Materials Science and Technology, Überlandstrasse 129, 8600 Dübendorf, Switzerland

Abstract

The evolution of real-time medical diagnostic tools such as angiography and computer tomography from radiography based on photographic plates was enabled by the development of integrated solid-state X-ray photon detectors, based on conventional solid-state semiconductors. Recently, for optoelectronic devices operating in the visible and near infrared spectral regions, solution-processed organic and inorganic semiconductors have also attracted immense attention. Here we demonstrate a possibility to use such inexpensive semiconductors for sensitive detection of X-ray photons by direct photon-to-current conversion. In particular, methylammonium lead iodide perovskite ($CH_3NH_3PbI_3$) offers a compelling combination of fast photoresponse and a high absorption cross-section for X-rays, owing to the heavy Pb and I atoms. Solution processed photodiodes as well as photoconductors are presented, exhibiting high values of X-ray sensitivity (up to 25 μC mGy_{air}^{-1} cm^{-3}) and responsivity (1.9×10^4 carriers/photon), which are commensurate with those obtained by the current solid-state technology.

Introduction

The detection of X-ray photons is of utmost importance for a wide field of applications, ranging from specific crystal structure determinations1 to radio astronomy.2 The largest demand for X-ray detectors comes from medical radiography, where pixel array detectors

* wolfgang.heiss@jku.at.

Author contributions

The manuscript was prepared through the contribution of all authors. S.Y., M.S., D. K. and J. S. performed the work with the photoconductors. S.S., H.A., G.M. and M.R. prepared and tested the solar cell devices. W.H., G.M., C.B. and M.K. planned and supervised the work and had major input in the writing of the manuscript.

Competing financial interests: The authors declare no competing financial interest.

Europe PMC Funders Author Manuscripts

based on solid-state semiconductors are under development as a replacement for radiographic films.3–5 Out of the two current approaches to X-ray imaging, indirect conversion by use of scintillators and direct conversion of X-ray photons into electrical current (*e.g.,* by photoconductivity), the latter approach is reported to enable higher resolution.4 While sensitive photoconduction is observable in various crystalline inorganic semiconductors under X-ray illumination, including amorphous Se,3,6 crystalline Si,7 and CdTe,3,7 very few of these materials can be deposited uniformly onto thin-film-transistor active-matrix-arrays needed for the read-out of the electronic signals in pixel array detectors4,5,8 below the temperatures at which deterioration of the active-matrix occurs. In this respect, solution-processed semiconductors such as those applied in photovoltaic and photoconducting devices operating in the visible or infrared spectral region9–12 may represent an appealing alternative, owing to their low-temperature, non-vacuum and large-scale deposition in the form of homogeneous films by inexpensive techniques such as ink-jet, slit and screen printing, spin-casting and spray-coating. Finding such solution-processable semiconductors with high photoconductivity under X-ray illumination is therefore a key prerequisite. Here we report that methylammonium lead triiodide ($MAPbI_3$, where MA is CH_3NH_3), a solution-processable organic-inorganic direct-gap semiconductor, can be used as a highly sensitive photoconductor for the direct conversion of X-ray photons into electrical current. Although solution processing at lower temperatures is generally thought to reduce the electronic quality of semiconductors due to structural imperfections, numerous reports providing evidence of the very high suitability of such lead halide perovskites for optoelectronic applications were recently presented. In particular, perovskite based solar cells have rapidly progressed to certified power conversion efficiencies of up to 20%.13–18 Thin films of $MAPbI_3$ have also been used in bright light-emitting-diodes,19 as a lasing medium,20 and in highly sensitive detectors operating in the visible spectral region.21

For X-ray detection, not only are the semiconducting properties of the active material important, but also is the nature of its atomic constituents. This is because X-ray absorbance scales with atomic number (Z) as Z^4 / AE^3, where A is atomic mass and E is the X-ray photon energy. Thus, the absorbance at photon energies of ~10 keV to 1 MeV, plotted in Figure 1a based on the atomic absorption coefficients22 of the individual constituents of $MAPbI_3$, is dominated by the contribution of the Pb ions. At these high energies, the absorption length is more than 2 orders of magnitude larger than in the visible range, even though Pb is the second heaviest, after Bi, stable element in the periodic table. Thus, the ability to fabricate uniform semiconducting films with unusually large thicknesses, on the order of 10-100 μm, is also a prerequisite for the optimization of X-ray detectors. In this study, such thicknesses are readily obtained by spray-coating solutions of $MAPbI_3$ dissolved in common polar solvents such as dimethylformamide (DMF, Figure S1).

In this proof-of-concept study, we successfully test two main device architectures: photovoltaic and photoconductive. Thin-film photovoltaic cells (photodiodes), in which charge separation is achieved by the built-in potential of a p-i-n junction, exhibit a specific X-ray sensitivity of 25 μC mGy_{air}^{-1} cm^{-3}, which is commensurate with the performance of conventional solid-state semiconductor materials. In externally-biased thick-film photoconductors, capable of absorbing a much larger portion of the incident X-rays, a

similarly high X-ray sensitivity is obtained. Overall, up to ~2×10^4 charge carriers are generated per each 8 keV photon from a conventional CuK_α X-ray tube.

Photovoltaic cells

When operated as solar cells, these devices take full advantage of the strong optical absorbance of the $MAPbI_3$ in the near-infrared and visible spectral regions (Figure 1a), as well as the rather high carrier mobility (Figure 1b) and long exciton diffusion lengths23–25 compared to those of other common solution-processed semiconductors. The beneficial transport properties are also related to the crystal structure of $MAPbI_3$ (Figure 1c) comprising 3-dimensionally interconnected PbI_6 octahedra, leading to a relatively narrow band gap (1.56 eV) and small effective masses of the electrons and holes.26 Furthermore, good crystallinity with large crystallite sizes (> 250 nm), seen as sharp peaks in their X-ray diffraction patterns (Figure S2), are also important attributes for efficient charge transport.

For the efficient operation of photovoltaic devices, an important condition is that the diffusion lengths of the minority carrier species should exceed the device thickness.23 Recently demonstrated lead halide perovskite solar cells clearly fulfill this condition, resulting in high power conversion efficiencies of up to 20%.17 To harvest sunlight efficiently, active layer thicknesses on the order of 300 nm are required, which match the absorption length (*i.e.,* inverse absorption coefficient, Figure 1a) of $MAPbI_3$ in the visible and near infrared spectral regions. The orders of magnitude higher absorption length in the X-ray spectral region, however, raises the question of whether solution-processed perovskite solar cells, that by default use rather thin absorbing layers, are applicable for the detection of X-rays at all. On the other hand, such photodiodes are nearly perfectly optimized for the efficient separation of photo-generated electrons and holes by the built-in electric potential. Therefore, we tested a p-i-n type $MAPbI_3$ based solar-cell with poly(3,4-ethylenedioxythiophene) polystyrene sulfonate (PEDOT/PSS) as the hole contact and the soluble fullerene-derivative phenyl-C61-butyric acid methyl ester (PCBM) as the electron contacts (see Figure 2a). Under AM1.5 illumination from a solar simulator, this device provided a power-conversion-efficiency of 10.4% (Figure 2b), proving the efficient collection of photo-generated carriers. We then subjected this fully operational photodiode to illumination with a pulsed X-ray source (75 keVp photon energy, ~ 37 keV on average); a clear primary photocurrent response was observed under short-circuit conditions (*e.g.,* without applying any bias). The solar cell measured the same 50 Hz pulse-train as is also detected by a commercial silicon photo-diode reference detector with the help of a cerium doped ytterbium aluminium garnet (YAG:Ce) scintillator sheet emitting at 530 nm (Figure 2c). The measured photocurrent density scales linearly with the averaged X-ray dose rate (Figure 2d) and provides averaged values of up to 25 nA/cm^2. These values can be recalculated as a specific sensitivity (in units of $\mu C\ mGy_{air}^{-1}\ cm^{-3}$), which is a figure of merit for X-ray detectors, by normalizing the averaged photo-current by the dose rate (in air), the active area, and the X-ray absorbing layer thickness. The resulting values (inset in Figure 2d) are competitive with those exhibited by amorphous Se, being the only photoconductor material applied in commercial clinical flat panel based X-ray imagers. The specific sensitivities of amorphous-Se, depending on the operating field and thickness, were reported to be in the range of 1 – 17 $\mu C\ mGy_{air}^{-1}\ cm^{-3}$,27,28 whereas values of up to 25 $\mu C\ mGy_{air}^{-1}$

Europe PMC Funders Author Manuscripts

cm^{-3} are obtained here. These results clearly demonstrate the great potential of $MAPbI_3$ for direct conversion of X-ray radiation into mobile carriers.

Photoconducting devices

While the photovoltaic structure provides a high specific sensitivity, which is a value normalized by the volume of the active material, a substantially improved response in the X-ray regime could be expected for devices with much thicker active layers, with absorption lengths of up to ~100 μm (Figure 1a). Since this value is substantially larger than the measured minority carrier diffusion lengths in $MAPbI_3$ (~1 μm),[23–25] a sufficiently high external bias must be applied to provide efficient charge separation. Under external bias, lateral device architectures are advantageous compared to vertical ones since they are free of delicate interfaces between electron and hole extracting/blocking layers which might lead to accelerated device degradation. Instead, they make use of two interdigitate gold contacts whose distance apart is approximately equivalent to the layer thickness (inset in Figure 3a). Since relatively high external fields are applied to such photoconductors, the device performance is mostly independent of the work function of the chosen electrode material, and is instead primarily dominated by the properties of the active layer. Thus, the main precondition for device preparation in this work is the ability to deposit uniform $MAPbI_3$ films with desired thicknesses on patterned electrode structures; this was accomplished by spin-casting to achieve layer thicknesses of up to 1-2 μm and by spray-coating to achieve much thicker films (10-100 μm, Figure S1).

Similarly to the experiments with photovoltaic devices, we first tested the utility of a $MAPbI_3$-based lateral photoconductor device for detecting photons in the visible spectral region. At these wavelengths, an optimal thickness of 1-2 μm was estimated as necessary to exceed the absorption lengths. The high photon sensitivity of such a device is already seen in its I-V characteristics (Figure S3). While in darkness a conductivity of about 1.4×10^{-9} S/cm is measured, this value increases by 4 orders of magnitude under white light illumination with an intensity of 20 mW/cm^2. Further, the responsivity spectrum, shown in Figure 3a, closely reproduces the features of the absorption spectrum. The responsivity exceeds a value of 1 A/W in almost the entire visible part of the light spectrum; this corresponds, by multiplication with the photon energy (800 nm is equivalent to 1.55 eV), to a product of external quantum efficiency times photoconducting gain of slightly above unity. Since the quantum efficiency is always < 1, with the only exception being the case of multi-exciton generation taking place at energies well above the band gap, the measured responsivity indicates the occurrence of low *photoconductive gain* in $MAPbI_3$. Gain is observed when the carrier lifetime exceeds the carrier transit-time and thus high gain is often associated with carrier trapping.[10] Carrier trapping usually results in a slowing of the detector's response. The photoconductors investigated herein, however, exhibit a very fast response. In particular, upon laser excitation with short 10 ps pulses from a mode-locked laser, a pulse response with a full width at half maximum of 350 ps is measured by a sampling oscilloscope (inset in Figure 3b). This short response time corresponds to a cut-off frequency of ~3 GHz, which is higher than the recently reported maximum band-width of 3 MHz in solution-processed perovskite photodetectors operated in the visible spectral region.[21] With $MAPbI_3$ being largely free of carrier trapping, the bandwidth is instead limited by the RC-constant of the

device, which is substantially smaller in the lateral device geometry leading to much faster operation as seen in this study.

Having established that $MAPbI_3$ is a fast and sensitive photoconductive material in the visible spectral region, we then investigated its response to X-ray photons. As previously discussed, to absorb a majority of the X-ray photons a device is exposed to, thicker active materials are required. For X-ray photoconductivity experiments, film thicknesses equal to or higher than the X-ray absorption length must be selected, which can be determined from the data presented in Figure 1a or from the experimental thickness-dependence of the transmittance (Figure S4). For a conventional CuK_α X-ray tube source (8 keV), this thickness is ~30 μm.

Under ambient conditions, a photoconductor consisting of a 60μm layer of $MAPbI_3$ exhibits a close to linear I-V curve in darkness (Figure 3c). Under X-ray irradiation of 1.4×10^7 photons/mm^2, at a bias across the electrodes of 80 V and with a spacing of 100 μm, a photocurrent density of 7 μA/cm^2 (40 nA photocurrent) was obtained, which is >100 times higher than the value obtained using photodiodes with sub-micrometer active layers. The detector's responsivity reached 1.9×10^4 carriers/photon. This high value is based on two contributions: impact ionization, known from electron dispersive X-ray detectors,29 and photoconducting gain. The theoretical multiplicity of impact ionization is given by the ratio of the X-ray photon energy to the ionisation energy of the absorbing $MAPbI_3$. Taking the latter value of 5 eV for PbI_2,31 the impact ionization could only account for 5×10^3 charge carriers per photon. Thus, there must be a contribution from photoconducting gain as well, which contributes to the observed sensitivity by a factor of at least 30. This value is clearly higher than that observed for the ~500 nm thick photoconductors under visible light illumination and indicates considerably more charge trapping for the 60 μm thick devices under X-ray illumination. This observation can have several origins including a less favorable electric field distribution in thick devices, trapping in highly excited states, a larger number of grain boundaries within the thicker films, and, most importantly, the much smaller density of photoinduced carriers in thicker devices. Trap induced photoconducting gain is in fact helpful for obtaining higher detector sensitivity, except in the case that it leads to very slow response times which is not observed in this study.

A desirable property of a detector is a linear response as a function of intensity, such as that shown in Figure 2d for the p-i-n diodes and in Figure S5 for the thick X-ray photoconductors, covering at least three orders of magnitude. Such a high dynamic range is promising for roentgenography (e.g., in medicine, security, *etc.*), representing one of the most important applications of X-rays.8,28 To test the applicability of $MAPbI_3$ devices for imaging, a single element photoconductor was used in this example, and various objects were x,y-scanned with the X-ray beam. As shown in Figures 3d-i, well resolved images could be obtained for several objects: e.g., the leaf of a house plant, a Kinder Surprise egg, and an electronic card (used as a tag to identify products at the checkout desk of a shop). In all cases the X-ray images reveal details of the interior of the object which are not externally apparent: e.g., the veins of the *Begonia obliqua L.* leaf, the contents of the Kinder Surprise egg (a small guitar), and the circuit connected to a near field RF antenna within the electronic card (see reference photos in Figure 3). The X-ray images presented show

sufficiently high contrast and dynamic range, with the spatial resolution limited only by the dimensions of the photodetector and the X-ray beam collimation.

In comparison to common X-ray detection technologies, typically based on elaborate high vacuum deposition techniques, direct low-cost and low-temperature solution processing enables a wide range of possible device architectures and applications (large area X-ray scanners, required in medical diagnostics and for customs examinations, flexible X-ray scanners applied directly on the irregular contours of patients, all-printed X-ray detectors, *etc.*). Nevertheless, certain properties of $MAPbI_3$-based detectors require further improvement, such as the mobility, μ, and lifetime, τ, given that the product μτ (the carrier range) is an important controlling factor for the sensitivity.27 This product is usually extracted from the bias dependence of the responsivity,30,31 which in this case provides a value of 2×10^{-7} cm^2/V (Figure S6). Values in the same range, between 4×10^{-7} – 1.3×10^{-6} cm^2/V, are also deduced from the measured mobility (Figure 1c) and photoluminescence lifetimes.26 While these values are already comparable to those reported for amorphous selenium8,32 (the major material used in commercial X-ray imagers), X-ray detectors based on $MAPbI_3$ such as presented herein might easily be improved in the future, *e.g.*, by compositional engineering (using mixtures of halides such as $MAPb(Br/Cl/I)_3$),15,17,23,24 by increasing the crystalline grain size,33 and/or by smoothening the perovskite surfaces and interfaces.

In summary, we have presented the novel concept of applying solution-processed semiconductors for the detection of X-rays in both photoconductive and photovoltaic (p-i-n junction) device architectures. The X-ray sensitivity achieved by $MAPbI_3$ p-i-n photodiodes is comparable to those of established X-ray detector materials. The $MAPbI_3$ photoconductors, fabricated and tested in ambient conditions, show almost ideal photoresponse in the near-infrared to visible range, with external quantum efficiencies close to 100% and fast response times corresponding to cut-off frequencies of 3 GHz. In thick-film (60 μm) photoconductors, ~100 fold higher photocurrent densities are observed under X-ray illumination than in the p-i-n diodes. This higher responsivity is achieved by matched layer thickness, and is partly caused by a moderate photoconducting gain. The low-temperature solution processing of $MAPbI_3$ from molecular precursors suggests great promise for facile integration into inexpensive industrial read-out electronics for imaging, applicable for scientific purposes and medical diagnostics.

Methods

Synthesis of $MAPbI_3$ perovskite

Chemicals. A methylamine solution (33 wt. %) in absolute ethanol, hydriodic acid (57 wt. %) in water (99.99% trace metals basis), and anhydrous diethyl ether were received from Sigma-Aldrich. Lead(II) iodide (99.9985%) and anhydrous N,N-dimethylformamide (DMF) were purchased from Alfa Aesar. Absolute ethanol was supplied by Merck. All chemicals were used as received.

MAI (CH_3NH_3I) was synthesized by a simple neutralization reaction between methylamine and hydriodic acid. Into 100 ml absolute ethanol, 35 ml of a methylamine solution (33 wt.

%) and 20 ml hydroiodic acid (57 wt. %) were added. The mixture was vigorously stirred and cooled to room temperature °C by a water bath. After 30 min the solvent was removed by a rotary evaporator and a brown crystalline powder was collected. The powder was washed with 100 ml of anhydrous diethyl ether, stirred together with the powder for 30 min. After decanting the solvent, the washing step was repeated. For final purification, the powder was refluxed with 100 ml of ethyl ether for 2 h. The dispersion was then cooled to -18°C and vacuum filtered through a Schott funnel. The final white powder was dried under vacuum for 24 h and stored under a nitrogen atmosphere. $MAPbI_3$ was prepared inside a glove box by mixing MAI and PbI_2 in a 1:1 molar ratio in anhydrous DMF.

Device preparation—The p-i-n photodiode consisted of four spin-casted layers (see Fig 2a). On top of a indium tin oxidecovered glass substrate (6 ohm/□), a hole conducting layer of PEDOT:PSS (~50nm, VP Al 4083 from Heraeus Clevios) was deposited, followed by a layer of light absorbing $MAPbI_3$ semiconductor. This perovskite layer was processed from either a 25, 30 or 40 wt% MAI:PbI_2 precursor solution in anhydrous DMF, and the resulting layer thickness was 260 ± 60 nm, 360 ± 80 nm and 600 ±120 nm, respectively. The film was annealed for at least 90 min at 90 °C. To finish the device stack, an electron/hole conducting/blocking phenyl-C61-butyric acid methyl ester (PCBM) layer (~100nm) was added, followed by a ZnO layer (~40nm, nanoparticular ZnO dispersion provided by Nano-grade Ltd.) and finally followed by a Ag top contact (~100 nm, thermal evaporation deposited). All processing steps were performed in a dry N_2 glovebox. For the preparation of photoconductors, a 40 wt% DMF solution was used. The solution was either spin-casted or spray-coated onto a glass substrate with interdigitate electrodes (Au/Ti with a width of 1.8 mm and distances between 10-100 μm, depending on the thickness of the perovskite layer). The perovskite layer was dried at 130°C for 15 min.

Material and device characterization—The active layer thickness was determined by atomic force microscopy (AFM, Dimension 3100 from Veeco). **Powder X-ray diffraction** was measured with a custom-built Huber diffractometer equipped with a rotating Cu anode (Bruker AXS M18XCE). A double-bent parabolic multilayer was used to provide a parallel beam and a one dimensional Bruker Vantec-1 detector was used for signal detection. **Absorption spectra** of $MAPbI_3$ layers were measured by a Vis-NIR integrating sphere. Illumination was performed with a tungsten lamp and the spectra were collected with an AvaSpec-2048-SPU spectrometer. **Photoconductivity** (PC) measurements were performed by illumination with a tungsten lamp, monochromatized by an Acton SP2150 (Roper Scientific) spectrograph/monochromator. The light was chopped at a frequency of 33 Hz and the sample bias was varied from 10-20 V. The signal was collected by a Stanford Research 830 lock-in amplifier. I-V characteristics were measured by the Keithley 236 SMU, with and without the illumination of a tungsten lamp. **Transient photoconductivity and time-of-flight** were measured under excitation with 10 ps laser pulses from a frequency doubled YAG:Nd laser, emitting at λ=532 nm (Duettino from Time-Bandwidth), with 1- 50 μJ pulse energies. The transients, averaged over 128 pulses, were recorded by a Tektronix 1102 digital oscilloscope with a 100 MHz bandwidth (TOF), or a Tektronix 11801C digital sampling oscilloscope equipped with a 20 GHz sampling head. The steady state **photo-**

current measurements of the p-i-n solar-cell were performed with a Keithley 2400 instrument under AM1.5 illumination from a Newport Oriel Sol1A solar simulator.

X-ray absorption and X-ray response were measured with the same instrument as for X-ray diffraction. A 1x1 mm^2 parallel beam of CuK_α radiation was obtained after a pair of crossed slits. A commercial diffractometer detector (Bruker Vantec-1) was used for calibration of the X-ray intensity. It was replaced by the $MAPbI_3$ photoconducting sample for its characterization. For the X-ray absorption imaging, the imaged objects were moved into the X-ray beam by a 2D scanner. All measurements were performed in complete darkness. The sample was biased with voltages up to 40 V across the electrode distance of 100 μm. The bias was applied by a Keithley 236 SMU and the chopped signal was recorded by a Stanford Research 830 lock-in amplifier. Control experiments were also made with plain electrodes (not covered by perovskites) to determine whether the photon currents were due to air-ionization by X-rays or other artifacts. All X-ray absorbance measurements were performed and all images were collected with the same $MAPbI_3$ photoconductor, held in ambient atmosphere; during all measurements, no degradation of the detector sensitivity was observed.

The pulsed photo-current of the p-i-n solar cell was recorded at 0 V bias with a FEMTO DLPCA-200 transimpedance amplifier and a Tektronix DPO-2024 oscilloscope. The pulsed X-ray source (Nanodor 1 from Siemens) was operated with a tungsten anode and 75 kVp (~37 keV averaged) acceleration voltage at 50 Hz. The X-ray dose was measured with an Iba Dosimax plus dosimeter and the attenuation of the X-ray exposure was achieved with a stack of 27 μm thick lead foils.

Supplementary Material

Refer to Web version on PubMed Central for supplementary material.

Acknowledgements

The authors thank the Austrian Science Fund FWF for financial support via the SFB project IR_ON. A part of the research was also performed at the Energie Campus Nürnberg and supported by funding through the “Aufbruch Bayern” initiative of the state of Bavaria. M.K. and S.Y. acknowledge partial financial support from the European Union through the FP7 (ERC Starting Grant NANOSOLID, GA No. 306733). The authors thank Violetta Sassi, Sonja Roters, Ekkehard Nusko, Wolfgang Grafeneder and Maryna Bodnarchuk for technical assistance. SY thanks Mike Hardman for assisting with the selection of plants for X-ray imaging. We thank Nicholas Stadie for reading the manuscript.

References

1. Tegze M, Faigel G. X-ray holography with atomic resolution. Nature. 1996; 380:49–51.
2. Shanmugam M, et al. Alpha Particle X-Ray Spectrometer (APXS) on-board Chandrayaan-2 rover. Adv Space Res. 2014; 54:1974–1984.
3. Yaffe MJ, Rowlands JA. X-ray detectors for digital radiography. Phys Med Biol. 1997; 42:1–39. [PubMed: 9015806]
4. Kasap SO, Rowlands JA. Direct-conversion flat-panel X-ray image sensors for digital radiography. Proc IEEE. 2002; 90:591–604.
5. Moy JP. Recent developments in X-ray imaging detectors. Nucl Instr Meth Phys Res. 2000; 442:26–37.

6. Zhao W, Rowlands JA. X-ray imaging using amorphous selenium: Feasibility of a flat panel self-scanned detector for digital radiology. J Med Phys. 1995; 22:1595–1604.
7. Oh KM, et al. Measurement of the electrical properties of a polycrystalline cadmium telluride for direct conversion flat panel X-ray detector. J Instrum. 2014; 9:P01010.
8. Kasap S, et al. Amorphous and polycrystalline photoconductors for direct conversion flat panel x-ray image sensors. Sensors. 2011; 11:5112–5157. [PubMed: 22163893]
9. Halls JJM, et al. Efficient Photodiodes from Interpenetrating Polymer Networks. Nature. 1995; 376:498–500.
10. Konstantatos G, et al. Ultrasensitive solution-cast quantum dot photodetectors. Nature. 2006; 442:180–183. [PubMed: 16838017]
11. Keuleyan S, Lhuillier E, Brajuskovic V, Guyot-Sionnest P. Mid-infrared HgTe colloidal quantum dot photodetectors. Nat Photonics. 2011; 5:489–493.
12. Rauch T, et al. Near-infrared imaging with quantum-dot-sensitized organic photodiodes. Nat Photonics. 2009; 3:332–336.
13. Chung I, Lee B, He J, Chang RP, Kanatzidis MG. All-solid-state dye-sensitized solar cells with high efficiency. Nature. 2012; 485:486–489. [PubMed: 22622574]
14. Gratzel M. The light and shade of perovskite solar cells. Nature Mater. 2014; 13:838–842. [PubMed: 25141800]
15. Green MA, Ho-Baillie A, Snaith HJ. The emergence of perovskite solar cells. Nat Photonics. 2014; 8:506–514.
16. Im JH, Jang IH, Pellet N, Gratzel M, Park NG. Growth of $CH_3NH_3PbI_3$ cuboids with controlled size for high-efficiency perovskite solar cells. Nature Nanotech. 2014; 9:927–932.
17. Jeon NJ, et al. Compositional engineering of perovskite materials for high-performance solar cells. Nature. 2015; 517:476–480. [PubMed: 25561177]
18. Zhou H, et al. Photovoltaics. Interface engineering of highly efficient perovskite solar cells. Science. 2014; 345:542–546. [PubMed: 25082698]
19. Tan ZK, et al. Bright light-emitting diodes based on organometal halide perovskite. Nature Nanotech. 2014; 9:687–692.
20. Xing G, et al. Low-temperature solution-processed wavelength-tunable perovskites for lasing. Nature Mater. 2014; 13:476–480. [PubMed: 24633346]
21. Dou L, et al. Solution-processed hybrid perovskite photodetectors with high detectivity. Nature Commun. 2014; 5:5404. [PubMed: 25410021]
22. Grodstein, GW. X-ray Attenuation Coefficients from 10 keV to 100 MeV. U.S. Department of Commerce, National Bureau of Standards; 1957.
23. Stranks SD, et al. Electron-hole diffusion lengths exceeding 1 micrometer in an organometal trihalide perovskite absorber. Science. 2013; 342:341–344. [PubMed: 24136964]
24. Wehrenfennig C, Eperon GE, Johnston MB, Snaith HJ, Herz LM. High charge carrier mobilities and lifetimes in organolead trihalide perovskites. Adv Mat. 2014; 26:1584–1589.
25. Xing G, et al. Long-range balanced electron- and hole-transport lengths in organic-inorganic $CH_3NH_3PbI_3$. Science. 2013; 342:344–347. [PubMed: 24136965]
26. Baikie T, et al. Synthesis and crystal chemistry of the hybrid perovskite (CH_3NH_3) PbI_3 for solid-state sensitised solar cell applications. J Mater Chem A. 2013; 1:5628–5641.
27. Kasap SO. X-ray sensitivity of photoconductors: application to stabilized a-Se. J Phys D: Appl Phys. 2000; 33:2853–2865.
28. Schieber M, et al. Thick films of X-ray polycrystalline mercuric iodide detectors. J Cryst Growth. 2001; 225:118–123.
29. Juška G, Arlauskas K. Impact ionization and mobilities of charge carriers at high electric fields in amorphous selenium. Phys Status Solidi A. 1980; 59:389–393.
30. Kabir MZ, Kasap SO. Charge collection and absorption-limited sensitivity of x-ray photoconductors: Applications to a-Se and HgI_2 . Appl Phys Lett. 2002; 80:1664–1666.
31. Street RA, et al. Comparison of PbI_2 and HgI_2 for direct detection active matrix x-ray image sensors. J Appl Phys. 2002; 91:3345–3355.

32. Masuzawa T, et al. Development of an amorphous selenium-based photodetector driven by a diamond cold cathode. Sensors. 2013; 13:13744–13778. [PubMed: 24152932]

33. Nie W, et al. High-efficiency solution-processed perovskite solar cells with millimeter-scale grains. Science. 2015; 347:522–525. [PubMed: 25635093]

Europe PMC Funders Author Manuscripts

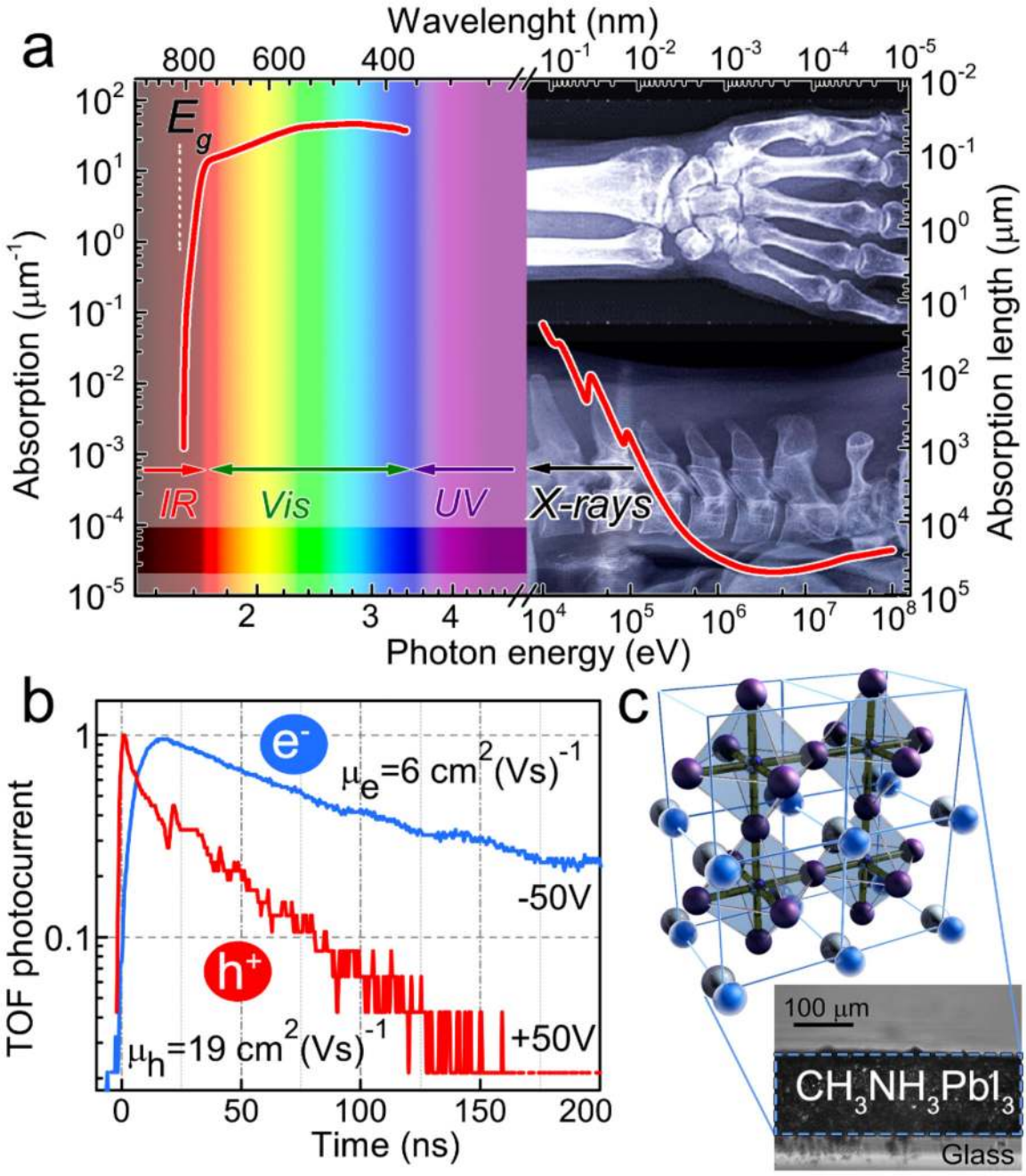

Figure 1. $MAPbI_3$ perovskite basic properties.

Absorption coefficient/length as a function of photon energy, covering the infrared to X-ray spectral region. (b) Time of flight transients for two bias directions, providing approximate electron and hole mobility. (c) Crystal structure of the perovskite: blue spheres – MA, black spheres – I, centers of the octahedrons – Pb. The inset shows a cross sectional micrograph of a spray coated $MAPbI_3$ layer.

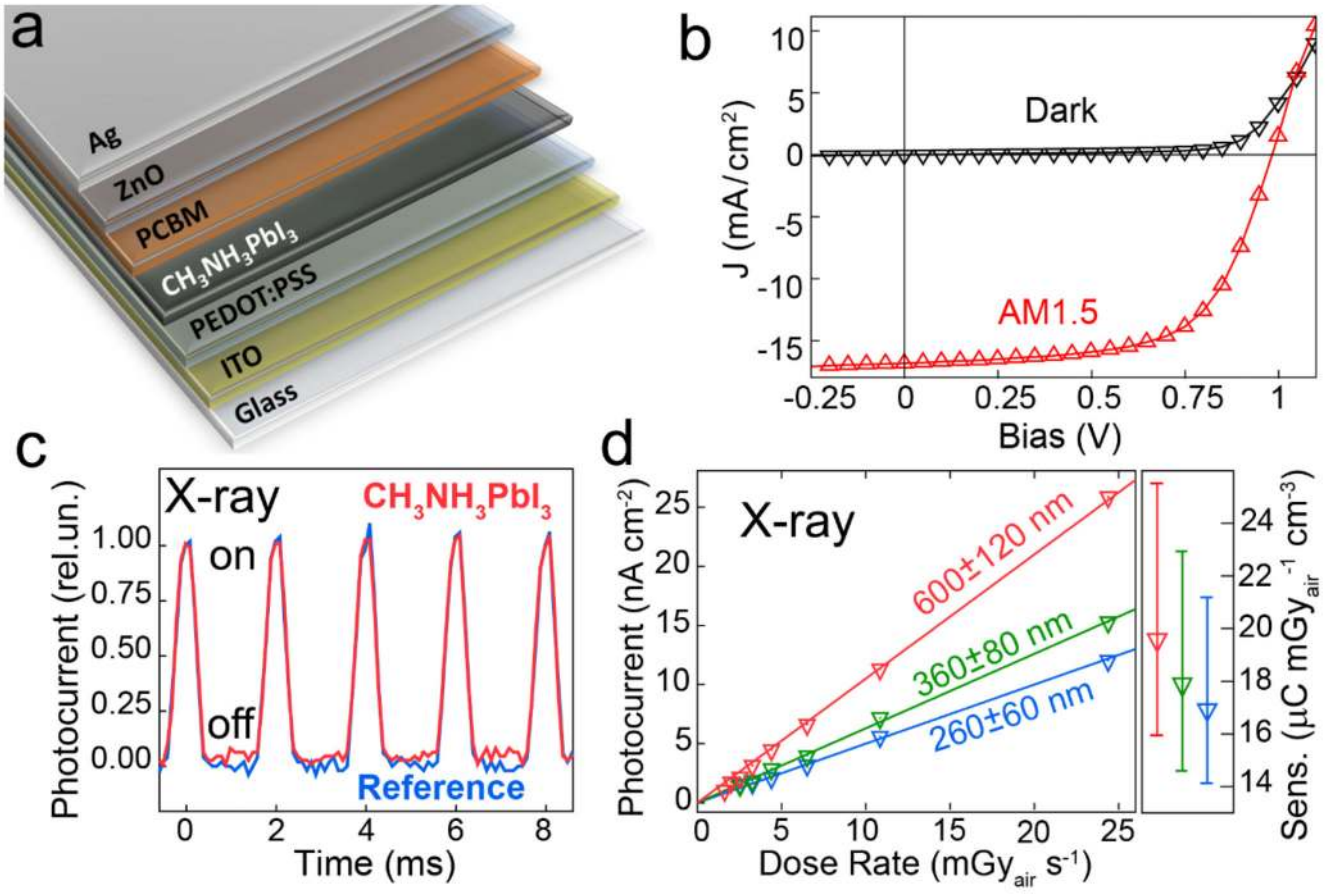

Figure 2. Photovoltaic device.

(a) Schematic of the layer stacking of the $MAPbI_3$ based p-i-n photodiode. (b) *JV* characteristics of the device in darkness and under AM1.5 illumination. (c) Time-resolved short-circuit photocurrent under X-ray exposure. The data shown in (b) and (c) are for a 260 ± 60 nm thick $MAPbI_3$ layer. (d) Averaged short-circuit X-ray photo-current as function of the dose-rate. In the inset, the sensitivity normalized to the active volume is given for 260 ± 60 nm, 360 ± 80 nm and 600 ±120 nm thick $MAPbI_3$ layers, respectively.

Europe PMC Funders Author Manuscripts

Europe PMC Funders Author Manuscripts

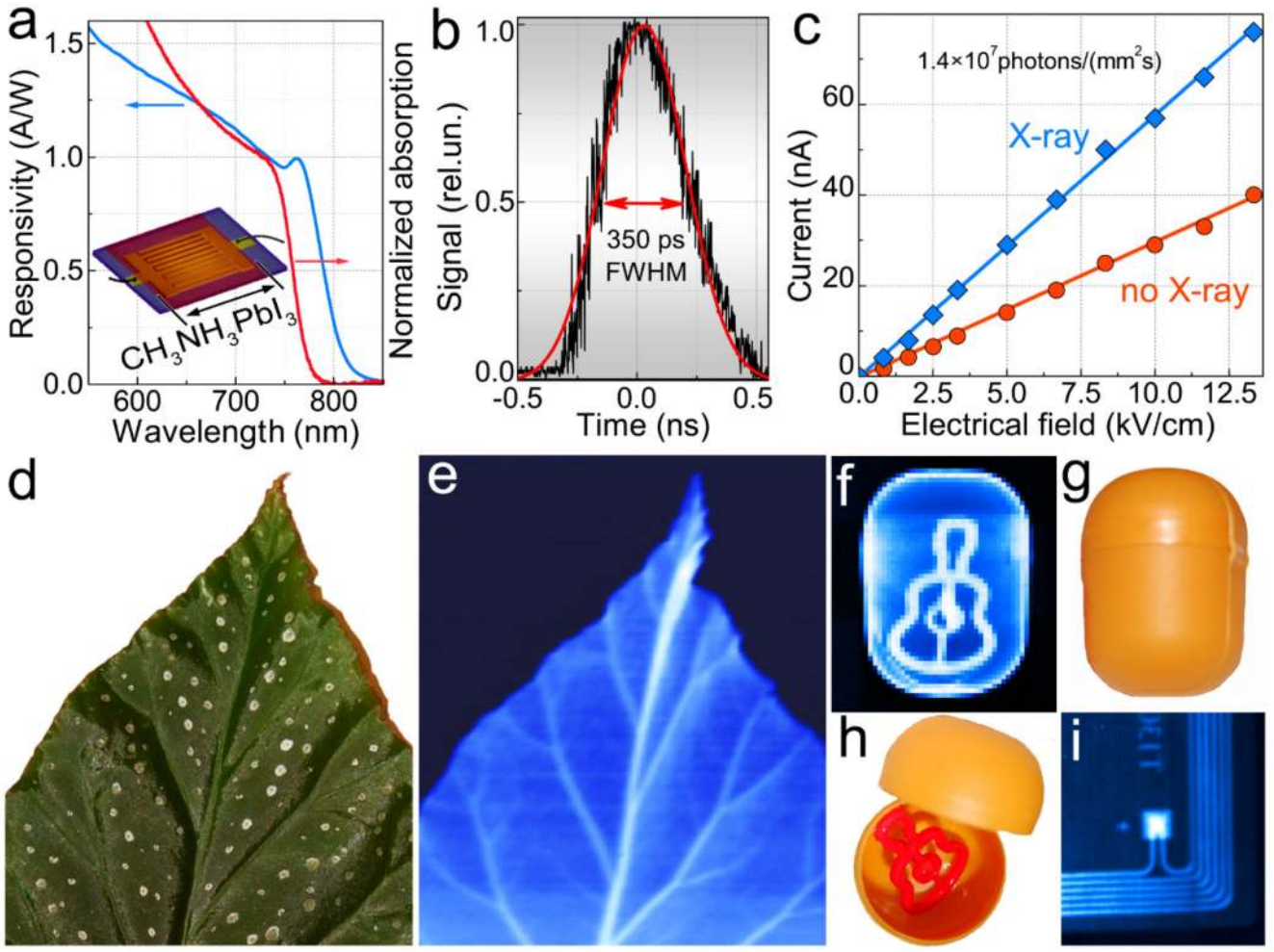

Figure 3. Visible and X-ray photoconductive devices.

(a) Responsivity- and absorbance- spectra of a 2 μm thick $MAPbI_3$ perovskite film in the visible spectral region. The inset shows the photoconducting device geometry with lateral interdigitate electrodes. (b) Photoresponse to a pulsed laser (10 ps, λ=532nm), providing a characteristic time at the full width at half maximum (FWHM) of 350 ps. (c) I-V characteristics of a 60 μm thick $MAPbI_3$ perovskite photoconductor in darkness and under X-ray illumination. (d) Photograph of a leaf (*Begonia obliqua L.*) and the corresponding X-ray image, (e), obtained with the photoconductor shown in (c). (f-i) X-ray images revealing the contents of a Kinder Surprise egg and the chip and RF-antenna integrated within an electronic key-card.